NASA TECHNICAL MEMORANDUM

NASA TM X-71799

NASA TM X-71799

(NASA TM-X-71799) POTENTIAL AND VISCOUS FLOW IN VTOL, STOL OR CTOL PROPULSION SYSTEM INLETS (NASA) 20 p HC $3.25 CSCL 01A

N75-32024

Unclas
G3/02 41113

POTENTIAL AND VISCOUS FLOW IN VTOL, STOL OR CTOL PROPULSION SYSTEM INLETS

by Norbert O. Stockman
Lewis Research Center
Cleveland, Ohio 44135

TECHNICAL PAPER to be presented at
Eleventh Propulsion Conference cosponsored by the
American Institute of Aeronautics and Astronautics and
the Society of Automotive Engineers
Anaheim, California, September 29 - October 1, 1975

POTENTIAL AND VISCOUS FLOW IN VTOL, STOL OR CTOL PROPULSION SYSTEM INLETS

Norbert O. Stockman*
Lewis Research Center
National Aeronautics and Space Administration
Cleveland, Ohio

Abstract

A method has been developed for analyzing the flow in subsonic axisymmetric inlets at arbitrary conditions of freestream velocity, incidence angle, and inlet mass flow. An improved version of the method is discussed and comparisons of results obtained with the original and improved methods are given. Comparisons with experiments are also presented for several inlet configurations and for various conditions of the boundary layer from insignificant to separated. The paper discusses applications of the method, with several examples given for specific cases involving inlets for VTOL lift fans and for STOL engine nacelles.

Introduction

Many proposed advanced aircraft, whether CTOL, STOL or VTOL, require propulsion system inlets to operate efficiently over wide ranges of flight speed, incidence angle and inlet throat Mach numbers (mass flow rates). These requirements can be quite severe for a fixed-geometry axisymmetric inlet. Therefore, considerable research and development effort is required for the design of such inlets.

The principal tool in inlet design has been wind tunnel experiments with scaled model inlets. Wind tunnel testing is both lengthy and expensive. To minimize the amount of wind-tunnel testing required and to ensure that reasonable geometries are tested, a reliable theoretical method of inlet analysis is needed. The method should be able to calculate the potential and viscous flow in inlets of arbitrary geometry and combinations of operating conditions.

Such a method has evolved over the past several years at the NASA Lewis Research Center. The original motivation for a potential flow analysis (ref. 1) was the need to design inlets for an in-house VTOL lift fan test program (refs. 2 & 3). The method was quite successful at this and was extended to several other applications (ref. 4). When the method was applied to STOL inlet designs, the boundary layer became significant, and the boundary layer or viscous calculations were incorporated into the system (ref. 5).

A status report on the resulting method as of late 1973 is given in reference 6. Since that paper, the method was improved and many additional applications were made (e.g., refs. 7 & 8). The present paper (essentially an update of ref. 6) will cover the elements of the method, a comparison of the improved method with the original method, several comparisons with experiment, and a discussion of number of design and analysis applications.

*Aerospace Engineer, V/STOL and Noise Division, Member AIAA.

Nomenclature

A, B, C	combination coefficients, eq (1)
C_f	local skin friction coefficient (ratio of wall shear stress to dynamic pressure at edge of boundary layer)
D	diameter
M	Mach number
P	pressure
S	surface distance
U_T	rotor tip speed
V	velocity
$\dot{W}$	inlet mass flow
α	inlet incidence angle
δ	boundary layer thickness
δ^*	boundary layer displacement thickness
Δ_i	change in rotor incidence angle
ρ	density
σ	source strength

Subscripts:

c	control station
cor	corrected for compressibility
cr	critical
h	highlight
i	incompressible
j	basic solution
max	maximum value
ref	reference value
s	static conditions
t	total or stagnation conditions
th	throat
∞	freestream value

Superscripts:

$\overline{\quad}$	average value
$\rightarrow$	vector quantity

Method of Solution

Statement of the Problem

The basic problem to be solved is to calculate the compressible viscous flow in an arbitrary axisymmetric inlet at any combination of operating conditions of inlet mass flow rate, $\dot{W}$, freestream velocity V_∞, and inlet incidence angle, α (fig. 1). At non-zero incidence angle the flow in and around the inlet is three-dimensional. At the present time there is no exact practical compressible viscous flow method of solution (computer program) capable of handling this inlet problem. Therefore, the problem is solved in several steps (shown schematically in fig. 2) as follows:

1. Geometry representation (Program SCIRCL)
2. Incompressible potential flow basic solutions (EOD)
3. Combined solutions with compressibility correction (COMBYN)
4. Boundary layer calculations (VISCUS)
5. Iterative loop

The four computer programs are available from COSMIC, Computer Center, Information Services, 112 Barrow Hall, University of Georgia, Athens, Georgia, 30602. Programs SCIRCL, EOD and COMBYN are one unit (ref. 9) with number LEW-12152; program VISCUS (ref. 5) is number LEW-12178. Each step will be next described in some detail.

Geometry Representation

The inlet is assumed to be axisymmetric and is represented by its meridional profile. This profile is broken into segments at convenient tangent points as shown in figure 3. Each segment may be defined by an analytic expression or a set of points. The inlet duct walls and the outer surface (nacelle or bellmouth) must be extended far downstream (fig. 3) to facilitate obtaining accurate potential flow solutions in the inlet region of interest. The geometry program (SCIRCL, fig. 2) prepares coordinate-point input for efficient use of the potential flow program and also prints out information such as curvature, wall angles, flow area distribution, etc., which is useful in preliminary screening of proposed inlet shapes.

Incompressible Potential Flow Basic Solutions

The Douglas-Neumann program (ref. 10) is used for calculating the incompressible potential flow. Briefly, the program utilizes a distribution of sources or sinks of initially unknown strength σ to represent the inlet profile. This representation results in an integral equation (see ref. 10 for details) which is exact for a continuous distribution of source strength. This continuous distribution is approximated by representing the inlet profile by a finite number of discrete elements characterized by a point on the element (e.g., the midpoint) called the control point. Each element has the same predetermined type of source strength distribution (e.g., constant, linear, parabolic). This approximation results in a set of linear algebraic equations that are solved by matrix methods for the source strength at the control points. Velocities at the control points and at specified off-body points are then calculated from the source distribution.

Method of approximation. Two methods of approximation have been used as shown in figure 4: (1) the original method, called the base method, which has been in use at NASA Lewis for several years; and (2) the improved method, called the higher order method which was recently put into use.

The base method (ref. 10) uses flat (linear) surface elements and assumes constant source strength over each element (fig. 4(a)). To obtain solutions of adequate accuracy this method often requires very large numbers of elements and consequent long computer times.

The higher order method (ref. 11) uses curved (parabolic) surface elements and assumes a linear variation in source strength over each element (fig. 4(b)). For a given accuracy this method requires fewer elements than the base method with consequent savings in computer time. Conversely, a greater accuracy can be obtained within the element-number limitations of a given program-computer system with this method.

Types of basic solutions. The Douglas potential flow program is used to obtain three basic solutions which are used in linear combination (to be explained under "Combined Solution" below) in order to satisfy the prescribed operating conditions (fig. 1). Two types of sets of basic solutions, as shown in figure 5, have been used at NASA Lewis. The first is the closed-duct method (in use for several years) and the second is the shroud-vorticity method (recently put into use).

The closed duct method uses a combination of a closed-duct inlet (fig. 5(a)) and an open-duct inlet both in an axial freestream flow to obtain a static arbitrary mass flow. This method has some shortcomings that will be illustrated later under "Comparison of Methods of Solution".

The shroud-vorticity method (fig. 5(b)) utilizes a distribution of unit vortices (in addition to the distribution of sources that represent the inlet profile) on the shroud surface to induce a static mass flow through the inlet. Any arbitrary static mass flow can be obtained by the use of a multiplicative factor. This method does not suffer the shortcomings of the closed-duct method.

Possible solution procedures. The two methods of approximation and the two methods of inducing static mass flow are independent of each other so that when they are used in all possible combinations there results four different procedures for the solution:

1. Higher order approximation - shroud vorticity.
2. Higher order - closed duct
3. Base method - shroud vorticity

4. Base method - closed duct

The effects of these four procedures are investigated in reference 12. In that reference the four methods are applied to both STOL and VTOL inlets at several operating conditions. The greatest difference in results (static pressure distribution) are obtained between method 1 (the method currently in use) and method 4 (original method) for thin-walled nacelle type inlets in static operation. An example is shown in figure 6. The differences are quite significant, with a particularly anomolous behavior for the old method in the region of the fan face. The location of the anomoly is the beinnning of the minimum thickness of the nacelle. The element size here is too large relative to the nacelle thickness. The anomolous behavior could be eliminated, and the curve of method 4 in figure 6 could be made to agree with that of method 1 by using a sufficiently large number of elements. However, for this particular inlet that number exceeds the limitations of the program. The conclusion from the investigation of reference 12, of which figure 6 is an example, is that the new method gives greater accuracy with fewer elements and consequent smaller computing time.

Combined Solution

The incompressible potential flow computer program just discussed is used to obtain three independent basic solutions (fig. 5). These three basic solutions $\vec{V}_i$, $i = 1,2,3$ are then combined (program COMBYN, fig. 2) into a solution of interest $\vec{V}$ having arbitrary flow conditions of V_∞, α, and mass flow $\dot{W}$ (fig. 1). The combination equation is:

$$\vec{V} = A\vec{V}_1 + B\vec{V}_2 + C\vec{V}_3 \qquad (1)$$

where A, B, and C are obtained from the three flow conditions. Thus, once the basic flow solutions are obtained for a specified geometry, any solution of interest for that geometry can be obtained without repeating the more time-consuming potential flow calculations.

Compressibility

The velocity obtained by equation (1) is incompressible and is corrected for compressibility by the Lieblein-Stockman compressibility correction (ref. 13).

$$V_{cor} = V_i \left(\frac{\rho_t}{\rho_s}\right)^{V_i / \bar{V}_i} \qquad (2)$$

where all the terms on the right hand side are obtained from the incompressible flow solution or the input flow conditions. This correction requires no alteration of the inlet geometry and it can handle local sonic and supersonic velocities. From the compressible velocity, V_{cor}, other flow properties (Mach number, pressure ratio, streamlines, etc.) are obtained.

Boundary Layer

The surface Mach number distributions obtained from program COMBYN are used as input to the Herring-Mellor boundary layer calculation (program VISCUS, fig. 2). Reference 5 contains a complete documentation of program VISCUS and references to the original sources. Program VISCUS calculates boundary layer profiles, displacement thickness δ^*, skin friction coefficient C_f, etc., at each station, and also predicts transition from laminar to turbulent flow. Separation (whether laminar or turbulent), is predicted when C_f is zero.

The boundary layer calculations are based on the assumption that the flow is two-dimensional, either planar or axisymmetric. Questions have been raised (e.g., by Schaub and by Presley and Perkins, DISCUSSION, of ref. 6) about the validity of using two-dimensional boundary layer calculations for flow that is three-dimensional. Up till now, the boundary layer calculations were made only along the inlet windward meridian (lower lip in fig. 1) because the longitudinal velocity gradients are most severe there and separation will occur there first. An attempt to assess the validity of using the two-dimensional boundary layer calculation along the windward and other meridians by comparing the calculated boundary profiles with experimental at several circumferential locations is currently nearing completion (ref. 14). In another approach, a study is underway to calculate the boundary layer along three-dimensional streamlines calculated from the potential flow on the inlet surface. This approach should result in the best approximation possible with the existing program system. Profiles calculated by this method will be compared with experimental data to assess the usefulness of this approach.

Another shortcoming of the boundary layer calculation is the neglect of shock interactions. Since many cases of current interest contain regions of local supersonic flow, it may be necessary to account for possible shock-boundary-layer interaction in the boundary layer calculations. Furthermore, the transition model is not able to predict separation bubbles that appear to be present in the experimental data especially in small-scale. However, it might be feasible to include the predictions of a separation bubble in an improved transition model.

Iterative Loop

If the boundary layer is significant in the inlet region of interest, it may be desireable to add the displacement thickness δ^* to the original inlet profile and repeat the entire solution procedure, thus obtaining a new Mach number distribution, new δ^*, etc. This process may be iterated to satisfactory convergence. Usually one iteration is sufficient. In parametric studies or preliminary design screening, often no iteration is needed.

Comparisons with Experiment

To indicate the accuracy of the various aspects of the prediction method several comparisons with experimental data will be given. These will range over incompressible flow, compressible flow with insignificant boundary layer, and compressible viscous flow with various conditions of the boundary layer.

Incompressible

The surface pressure distributions in a chordwise cut of a VTOL fan-in-wing inlet at low forward velocity are shown in figure 7. The experimental data of figure 7 were obtained from the National Research Council of Canada (ref. 15). Three surfaces are shown on the plot: the forward surface of the bellmouth; the centerbody; and the aft surface of the bellmouth. The agreement between theory and experiment is quite good everywhere on the inlet. This case is included to illustrate the adequacy of the method of geometry representation even when the calculational model (see fig. 3(b)) differs rather significantly from the real geometry.

Compressible

The next case illustrates the applicability of the method when the flow is compressible. Figure 8 shows the theoretical and experimental surface pressure distributions on a VTOL fan-in-pod inlet (ref. 3). Both incompressible and incompressible-corrected-for-compressibility theoretical curves are given. The experimental static pressures agree quite well with the theory corrected for compressibility along the entire surface of the inlet.

This good agreement when the flow is compressible is usually obtained with other configurations both VTOL and STOL, and at various operating conditions provided there are no extended regions of local supersonic flow. That there may be disagreement when there is supersonic flow is not surprising since the relation between local streamtube area and velocity is different for supersonic and subsonic flows and the method is based on the subsonic relation. Furthermore, there may be other real flow effects present in a supersonic flow not accounted for in the analysis such as the presence of shocks or shock-boundary-layer interaction.

To illustrate the kind of agreement that can be expected when regions of local supersonic flow are present, two examples will be given of STOL engine inlets. First a model STOL engine inlet at approach operating condition is shown in figure 9. The figure shows a comparison of calculated and measured static pressures on both the windward and leeward sides of the inlet. The agreement would probably be quite adequate for most design or analysis applications.

Another small scale model STOL engine inlet operating at a takeoff throat Mach number of 0.78 (for noise reduction purposes) in a 34-knot crosswind ($\alpha = 90^{\circ}$) is shown in figure 10. Here, although the theory follows the data in a general way, there are two regions of disagreement: (1) on the lip; and (2) in the rearward portion of the diffuser. The disagreement in the diffuser is due to neglecting the boundary layer thickness in the calculations (as will be seen in the next section). The disagreement in the region of the internal lip may be due to the presence of a separation bubble near the highlight and a shock (or compression waves) near the throat.

It should also be remembered that the observed disagreements between theory and small-scale wind tunnel experiments are not necessarily the fault of the theory. There may be errors in the measurements, model contours, wind tunnel wall effects or other induced effects. For example, in some cases of poor agreement between theory and experiment, the agreement could be improved markedly by inputing into the calculation an incidence angle two or three degrees different from the measured value, thus indicating a possible induced effect in the wind tunnel tests. In fact, a slight increase in incidence angle would improve the agreement on both windward and leeward sides of the inlet of figure 9.

Viscous (Boundary Layer)

A small-scale translating-centerbody sonic inlet in the retracted (cruise) configuration (fig. 11(a)) is used for comparing theoretical results including boundary-layer effects to experimental data. Various conditions of the boundary layer are obtained by varying the inlet incidence angle α of the model. In all cases, the one-dimensional throat Mach number is 0.50 and the freestream Mach number is 0.13 (These results are all taken from ref. 8.)

Boundary layer attached. Surface Mach number distributions for zero incidence angle are shown in figure 11(b). Two theoretical curves are shown to illustrate the effect of the calculated boundary layer on the surface Mach number. The solid curve is the potential flow (no δ^* correction); the broken curve is the potential flow obtained with δ^* added to the inlet profile. With δ^* added, there is an excellent agreement with the theory in the diffuser region. No separation is indicated either by theory or by experiment.

Diffuser separation. Results are shown in figure 11(c) for an incidence angle of 40°. Here the theory, with or without the δ^* correction, predicts separation in the diffuser at about the same point as the experimental data indicate the start of a "pressure plateau" commonly associated with an actual separation.

Lip separation. On figure 11(d) results are given for an inlet incidence angle of 50°. The theoretical Mach number distribution is what would be obtained if the inlet flow did not separate. The experimental data clearly indicate separation on the inlet lip. The theory also predicts lip separation, and although possibly not at the exact point as the actual separation, it is quite adequate as a guide in inlet design.

In cases where the theory predicts separation the calculations stop and there is no δ^* calculated beyond the point of separation. For cases where a δ^* correction is used, the distribution of δ^* into the separated region can be obtained by extrapolation using an unseparated case (lower α) as a guide (see ref. 8).

Additional comparison for this and other configurations can be found in reference 8. On the basis of these results, the theory seems adequate in predicting the boundary layer behavior for this type of inlet configuration.

Applications

The calculation method has been used in many applications. Among them are: design of inlets for test models; analysis of existing inlets; parametric studies to aid in future design work; and test support. Examples of test support are calibration of inlets for mass flow rate measurement and interpretation of experimental results by comparison with the calculated results.

In this paper several applications of the calculation method will now be discussed, some utilizing only the potential flow part of the calculation and others using also the boundary layer calculations.

Potential Flow

VTOL inlets. Two applications of the method to VTOL inlets will be discussed: one a design application; the other an analysis application.

An example of the use of surface velocity distributions and passage velocity profiles in the design of a VTOL fan-in-pod inlet is shown in fig. 12. The specific problem in this case is the determination of a near-optimum location of the point of tangency between the bellmouth and the pod surface. Three locations of this tangent point are shown in the inset in fig. 12(a). The theoretical surface velocity distributions on the three different bellmouths are also shown for both static and crossflow operation. It can be seen that both the velocity peaks and the unfavorable velocity gradients in crossflow are reduced as the tangent point is moved out to a larger radius. Thus case C would be expected to have the best crossflow performance. However, at static conditions case C shows a higher velocity peak and a more adverse velocity gradient than cases A and B. In order to select a best shape a compromise may be made between the static and crossflow operation.

The radial velocity profiles at the fan face are shown in fig. 12(b) for both static and crossflow conditions. The differences between the three cases were not significant enough to affect the choice. However, another application of the method can be pointed out here, namely that the calculated static velocity profile as well as the upstream streamlines can be used as input to the fan rotor design.

A second example (fig. 13) is the calculation of VTOL rotor inflow distortion in crossflow for the fan-in-wing configuration shown. The rotor of the fan and the inlet were both designed for static operation with a ratio of tip speed U_T to fan axial velocity V_c of 1.7. If this inlet is operated at a ratio of crossflow velocity to fan axial velocity of around 0.4, the incidence angle of the potential flow relative to the rotor blades will deviate from the design value by magnitude Δ_i, as indicated by the contours in figure 13. It can be seen that, in the plane of the rotor inlet, the incidence angle distortion due to the potential flow alone can be severe. (The incidence angle distortion as calculated does not include inlet total pressure variations or the modification of the potential flow due to the presence of the rotor.) The effect of potential flow inflow distortion on fan stage performance is illustrated in reference 2. Additional sets of calculated incidence contours can be obtained to study the effect of different design parameters such as inlet depth, transition velocity, inlet profile, and rotor tip speed.

STOL inlets. The next two applications are taken from a theoretical screening study of inlets for the Quiet Clean Short-Haul Experimental Engine (QCSEE) Project (ref. 7). The first is a study of the effect of varying internal-lip contraction ratios and the second is a study of the effect of external forebody shape on the internal flow.

The first example study was undertaken to ensure that a reasonable range of contraction ratios was chosen for experimental evaluation. Figure 14 shows the effect of the internal lip contraction ratio, $(D_h/D_{th})^2$, on the surface Mach number distribution at QCSEE takeoff conditions ($M_{th} = 0.79$, $M_\infty = 0.12$, $\alpha = 50^\circ$). The figure shows that the higher the contraction ratio, the better the Mach number distribution, i.e., the lower the peak value and the less severe the unfavorable gradient. (However, the takeoff performance must be compromised with the cruise performance, and the highest contraction ratio lip may not be best overall.)

The second example taken from the QCSEE study of reference 7 is the effect of external forebody bluntness on the peak Mach number in the internal lip surface (fig. 15). Two of the internal lips of figure 14 (with contraction ratios of 1.46 and 1.56) were studied with three different external forebodies. The external forebodies are characterized herein only by their value of bluntness. Bluntness is a parameter which takes into account the local bluntness of the forebody near the highlight, the aspect ratio of the forebody, and the relative scale of the forebody thickness to the highlight radius. (For details of the forebody contour and the quantitative definition of bluntness see ref. 7) These combinations were analyzed at two different operating conditions as shown on figure 14. At the QCSEE takeoff conditions (fig. 15(a)), the peak Mach number is quite sensitive to external forebody bluntness with the lower contraction ratio (1.46) lip being more sensitive than the 1.56 lip. However, at conditions more representative of CTOL takeoff, i.e., an incidence angle of 30° and a freestream Mach number of 0.18 (fig. 15(b)), the internal lip peak Mach number is essentially independent of external forebody bluntness.

Viscous Flow

The two principal uses of the boundary layer calculations in inlet analysis have been to obtain a more realistic potential flow solution by accounting for the displacement thickness, and to predict boundary layer separation. These uses have already been illustrated in the comparison with experiment in figure 11. The criterion for boundary layer separation in the method is that the local skin friction coefficient C_f go to zero. Two uses of the skin friction coefficient distribution will be discussed in this section: one illustrating the effect of incidence angle on distribution of C_f; the other illustrating the effect of scale.

Effect of incidence angle. Figure 16 (taken from ref. 8) shows the effect of varying incidence angle on the skin friction distribution of the inlet of figure 11. A local minimum with a low value of C_f is a point of likely separation as the operating conditions become more severe. The zero incidence curve indicates two regions of possible boundary layer separation (at the two minimums), one in the diffuser (where the flow is turbulent) and the other on the internal lip (where the flow is initially laminar). (The rise in C_f from the first minimum is due to the transition from laminar to turbulent flow.)

At an incidence angle of 20°, separation is indicated in the diffuser. As incidence angle is increased further up to 40° the separation point moves upstream somewhat but remains in the diffuser at a position close to the diffuser wall inflection point (S = 0.6). At the same time, the minimum on the lip decreases toward zero. Eventually, at 50° incidence, the separation point occurs at the lip as the minimum reaches zero there. That lip separation is predicted by the first minimum going to zero rather than the second minimum moving forward has been verified by taking very small increments in incidence angle (ref. 16). In reference 16 it was found that the forward movement of the diffuser separation location eventually stops and further increases in incidence angle reduce the lip minimum until it reaches zero indicating separation.

Experimental results correlating total pressure loss with separation location (ref. 8) for this inlet indicate that diffuser separation in the region of S = 0.6 leads to only small losses, whereas lip separation leads to intolerable losses. Thus, it appears that a distribution of C_f, like that of figure 16, is undesireable and if possible the inlet design should be modified to raise or eliminate the minimum on the lip.

Scale effects. The skin friction distribution is used in reference 17 to investigate the effects of scale on boundary layer separation prediction. Figure 17 (taken from ref. 17) shows the skin friction distribution for the inlet geometry of figure 10 at several different scales. The smaller the scale, the more likely is the boundary layer to separate. If the scale were made sufficiently small, the separation point would occur at the lip as in the case of increasing angle of attack (fig. 16).

The scale effects shown in figure 17 do not include the effects of scale on possible shock-boundary layer interaction or on more complex transition mechanisms (such as laminar separation with turbulent reattachment), since these effects are not currently included in the boundary layer program. The effects of longitudinal curvature on transition or boundary layer eddy viscosity are also not included in these particular calculations.

Figure 17 and other results of reference 17 indicate that testing at small scale tends to give pessimistic estimates of boundary layer behavior. An attempt will be made in reference 17 to provide a procedure for predicting boundary layer at full scale based on a combination of small scale test results and an improved version of the boundary layer calculations.

Concluding Remarks

A method for the prediction of potential and viscous flow in subsonic axisymmetric propulsion system inlets at arbitrary incidence angle and flow conditions has been developed. The method has already proven to be a very useful and powerful tool for both analysis and design purposes. The various elements of the method are constantly being updated, thus improving both its versatility and accuracy. It is probably the best tool available at present for analyzing the compressible viscous flow in axisymmetric subsonic inlets at arbitrary incidence angle and probably will continue to be until exact three-dimensional compressible inlet flow computer programs become practical.

References

1. Stockman, N. O.; and Lieblein, S.: Theoretical Analysis of Flow in VTOL Lift Fan Inlets Without Crossflow. NASA TN D-5065, 1969.

2. Lieblein, S.; Yuska, J. A.; and Diedrich, J. H.: Performance Characteristics of a Model VTOL Lift Fan in Crossflow. Journal of Aircraft, Vol. 10, No. 3, March 1973, pp. 131-136.

3. Stockman, N. O.; Loeffler, I. J.; and Lieblein, S.: Effect of Rotor Design Tip Speed on Aerodynamic Performance of a Model VTOL Lift Fan Under Static and Crossflow Condition. Journal of Engineering for Power, Trans. ASME, Series A, Vol. 95, No. 4, Oct. 1973, pp. 293-300.

4. Stockman, N.O.: Potential Flow Solutions for Inlets of VTOL Lift Fans and Engines. Analytical Methods in Aircraft Aerodynamics, NASA SP-228, Wash., D.C., 1970, pp. 659-681.

5. Albers, J. A.; and Gregg, J. L.: A Computer Program to Calculate Laminar, Transitional and Turbulent Boundary Layers for Compressible Axisymmetric Flow. NASA TN D-7521, 1974.

6. Albers, J. A.; and Stockman, N. O.: Calculation Procedures for Potential and Viscous Flow Solutions for Engine Inlets. Trans. ASME, Journal of Engineering for Power, Vol. 97, Series A, No. 1, Jan. 1975, pp. 1-10.

7. Albers, J. A.; Stockman, N. O.; and Hirn, John J.: Aerodynamic Analysis of Several High Throat Mach Number Inlets for the Quiet Clean Short-Haul Experimental Engine. NASA TM X-3183, January 1975.

8. Felderman, E. John; and Albers, J. A.: Comparison of Experimental and Theoretical Boundary-Layer Separation for Inlets at Incidence Angle at Low-Speed Conditions. NASA TM X-3194, February, 1975.

9. Stockman, N. O.; and Button, S. L.: Computer Programs for Calculating Potential Flow in Propulsion System Inlets. NASA TM X-68278, 1973.

10. Hess, J. L.; and Smith, A. M. O.: Calculation of Potential Flow About Arbitrary Bodies. Progress in Aeronautical Sciences, Vol. 8, O. Kuchemann, ed., Pergamon Press, 1967, pp. 1-138.

11. Hess, J. L.; and Martin, R. P.: Improved Solution for Potential Flow About Arbitrary Axisymmetric Bodies by the Use of a Higher-Order Surface Source Method. NASA CR-134694, July 1974.

12. Stockman, N. O. and Pinsoneault, K. S.: Evaluation of Several Solution Procedures Using Surface-Source Methods of Calculating Potential Flow in Propulsion System Inlets. NASA TM X to be published.

13. Lieblein, S.; and Stockman, N. O.: Compressibility Correction for Internal Flow Solutions, Journal of Aircraft, Vol. 9, No. 4, April 1972, pp. 312-313.

14. Boles, Michael A.; Stockman, Norbert O.; and Luidens, Roger W.: Comparison of Predicted and Measured Boundary Layer Profiles at Several Circumferential Positions in a STOL Inlet at Angle of Attack. NASA TM X to be published.

15. Schaub, U. W.: Experimental Investigation of Flow Distortion in Fan-In-Wing Inlets. Journal of Aircraft, Vol. 5, Sept-Oct. 1968, pp. 473-478.

16. Chou, David C.; Luidens, Roger W.; and Stockman, Norbert O.: An Investigation of Separation Prediction in a STOL Engine Inlet. NASA TM X to be published.

17. Chou, David C.; Stockman, Norbert O.; and Luidens, Roger W.: Scale Effects on Separation Prediction in a STOL Engine Inlet. NASA TM X to be published.

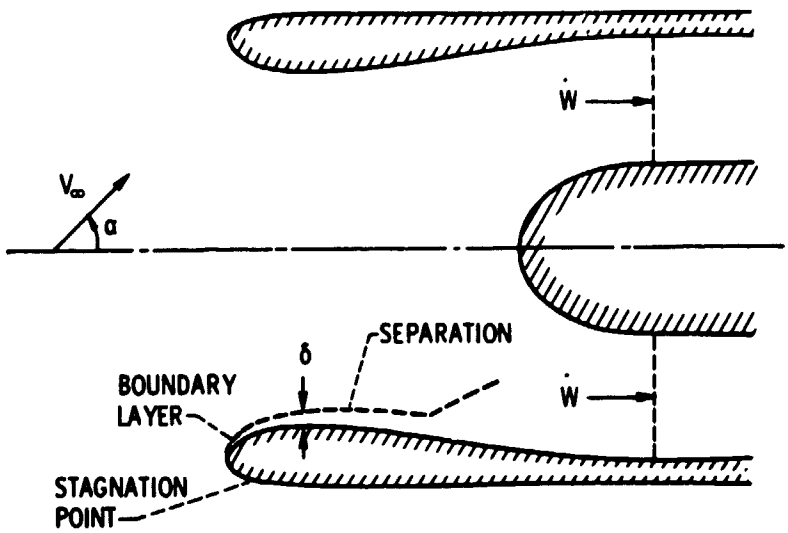

(a) CTOL OR STOL ENGINE INLET.

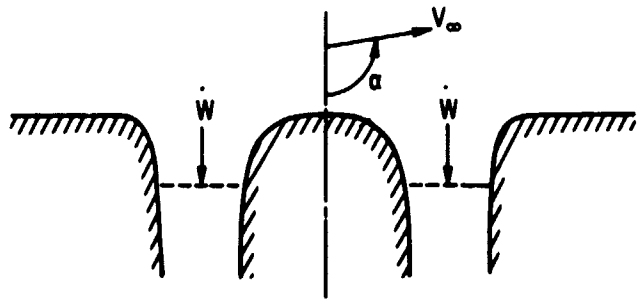

(b) VTOL ENGINE INLET.

Figure 1. - Inlet geometry and flow conditions: inlet mass flow rate, $\dot{W}$; free stream velocity, V_∞; and inlet incidence angle, α.

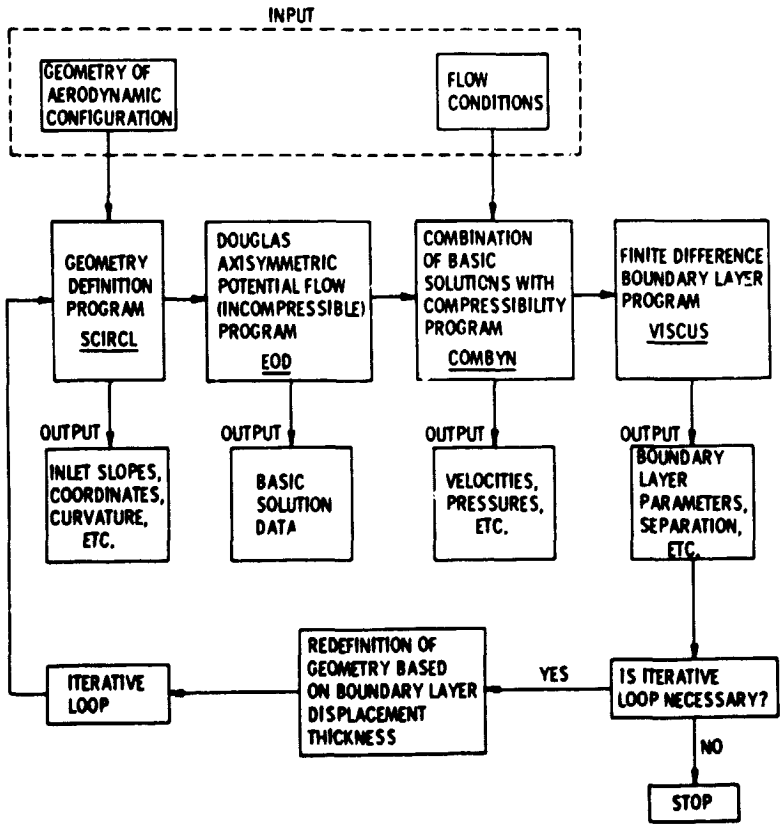

Figure 2. - Schematic of inlet programs.

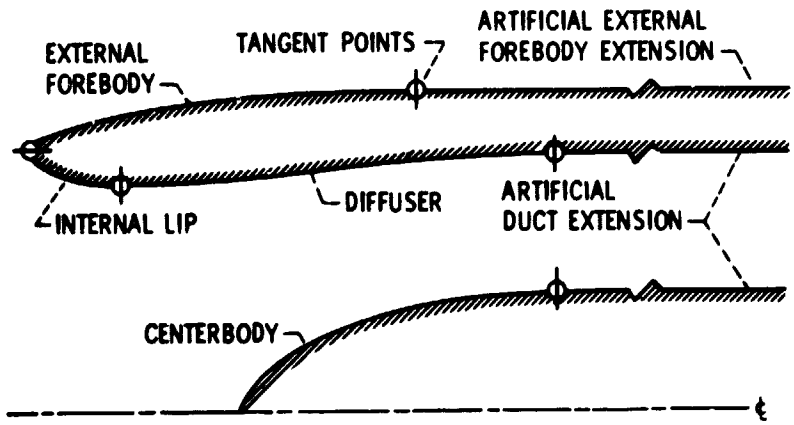

(a) CONVENTIONAL INLET.

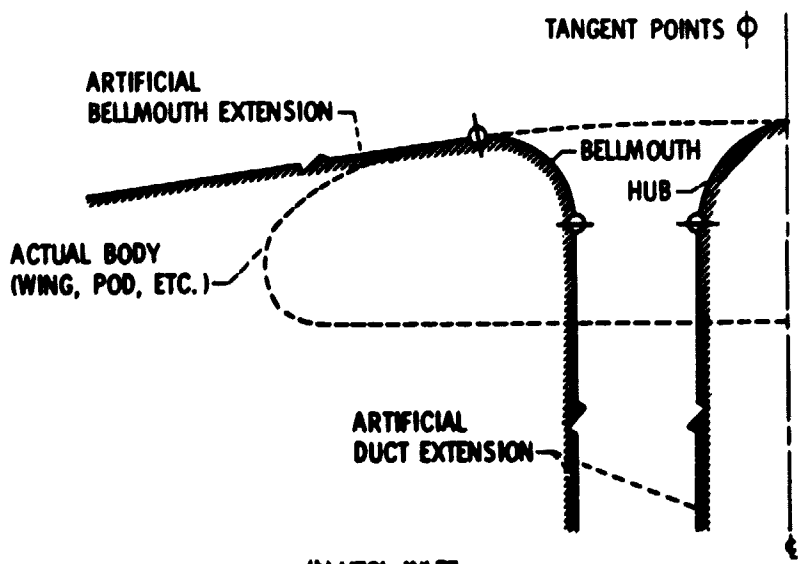

(b) VTOL INLET.

Figure 3. - Representative inlet geometries for potential flow solutions.

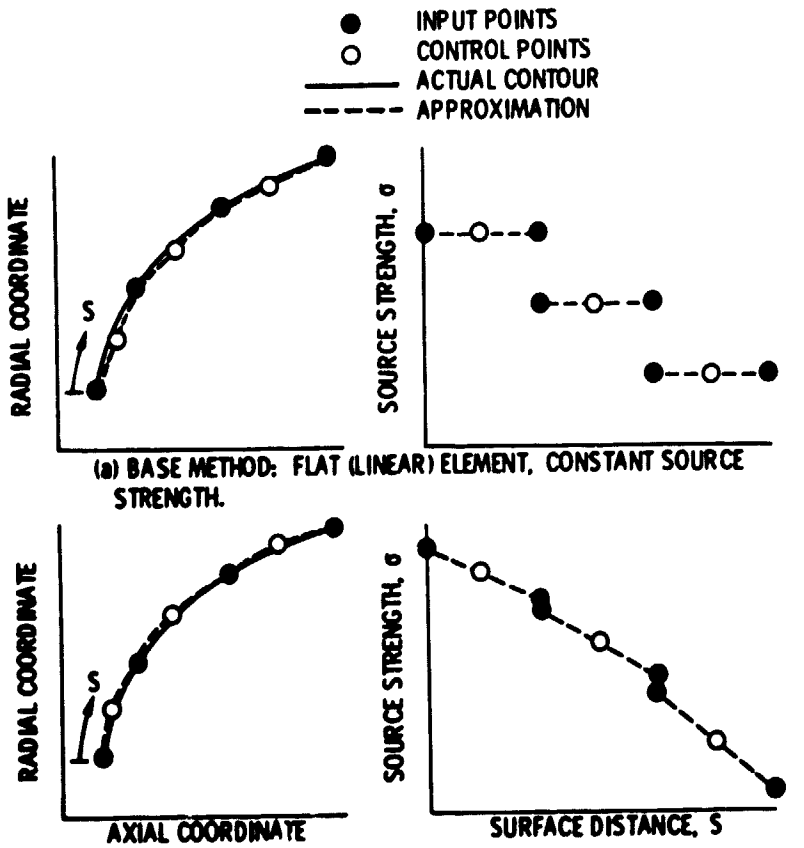

Figure 4. - Methods of approximating body surface contours and element source variation for basic solutions.

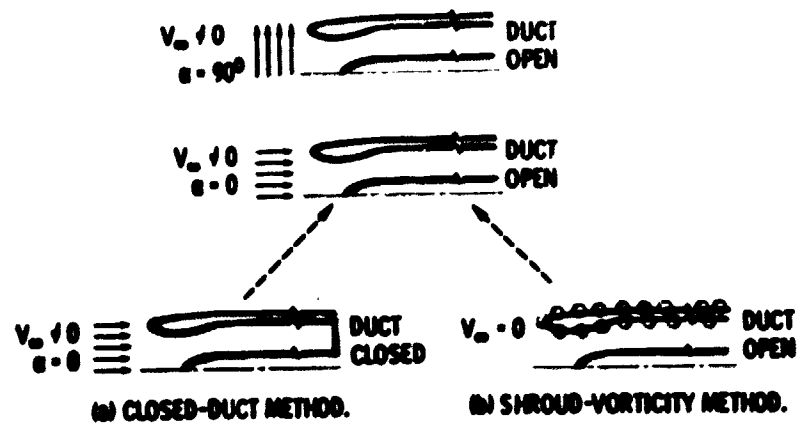

Figure 5. - Types of basic solutions considered.

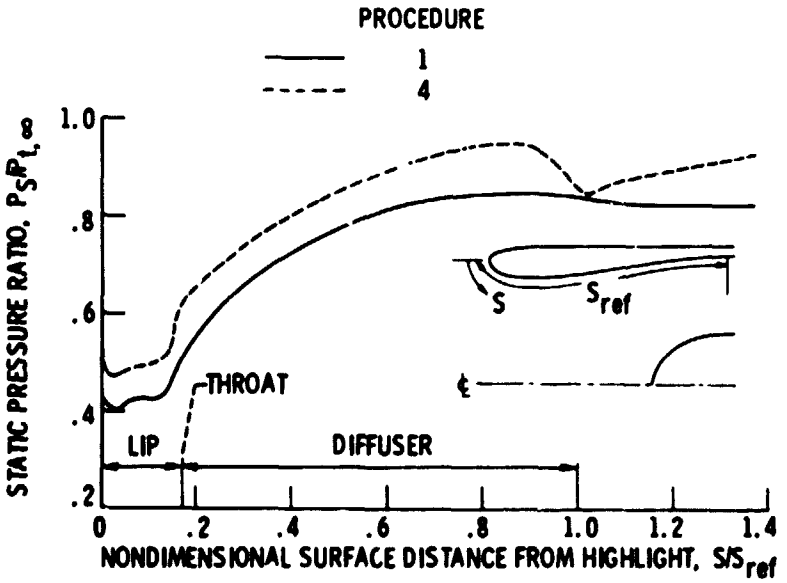

Figure 6. - Effect of solution procedure on pressure distribution on a STOL engine inlet. Static condition ($M_\infty = 0$), $M_{th} = 0.77$.

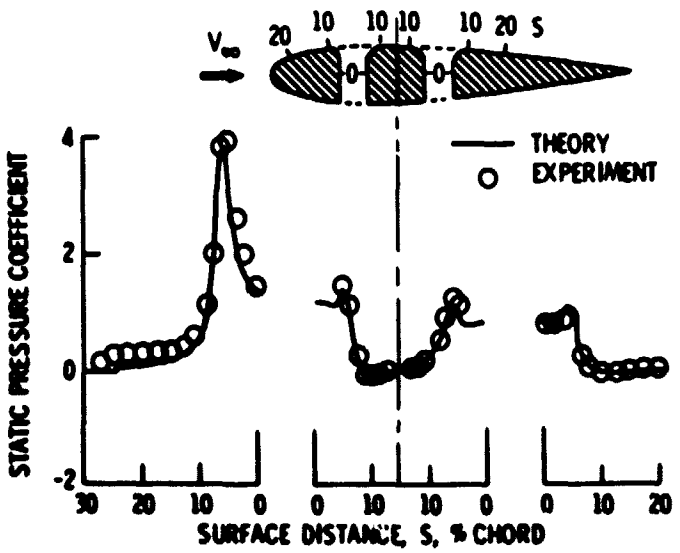

Figure 7. - Comparison with experiment of fan-in-wing surface pressure distribution. Average rotor inlet Mach number, $\overline{M}_t = 0.19$, $M_\infty = 0.05$.

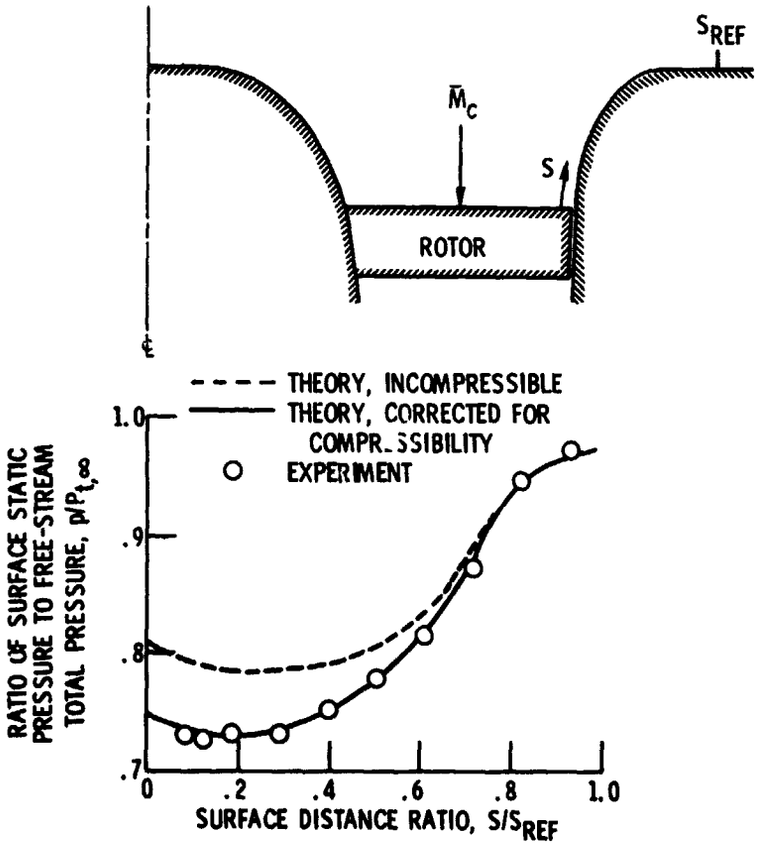

Figure 8. - Comparison with experiment of fan-in-pod inlet surface pressure distribution. Static condition, $V_\infty = 0$. Average rotor inlet Mach number, $\bar{M}_c = 0.57$.

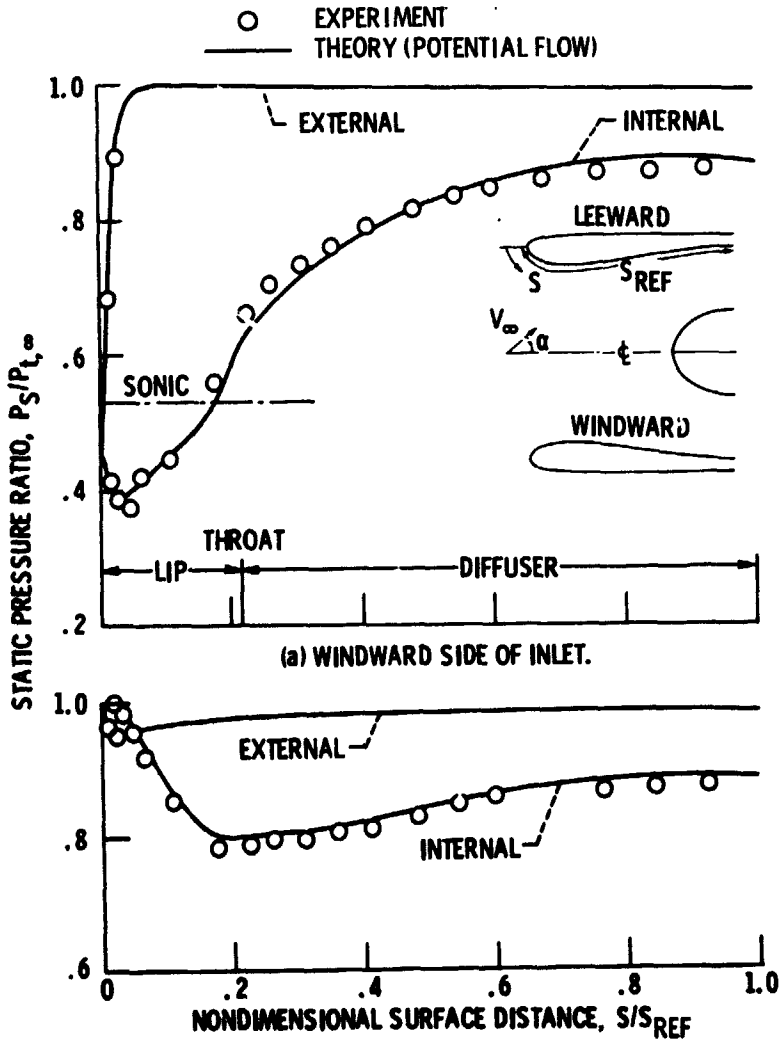

Figure 9. - Comparison with experiment for a STOL engine inlet at approach conditions. $M_{th} = 0.6$, $M_\infty = 0.18$, $\alpha = 40^0$.

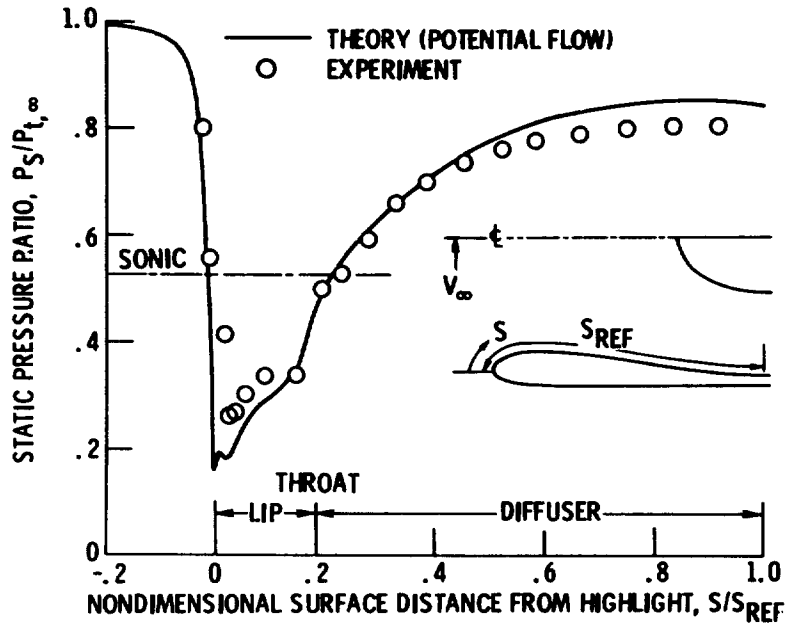

Figure 10. - Comparison of theory with experiment on windward side of a STOL engine inlet in a 90^0 crosswind. $M_{th} = 0.78$, $M_\infty = 0.05$, $\alpha = 90^0$.

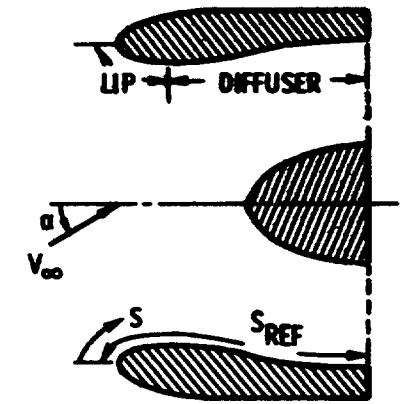

(a) GEOMETRY.

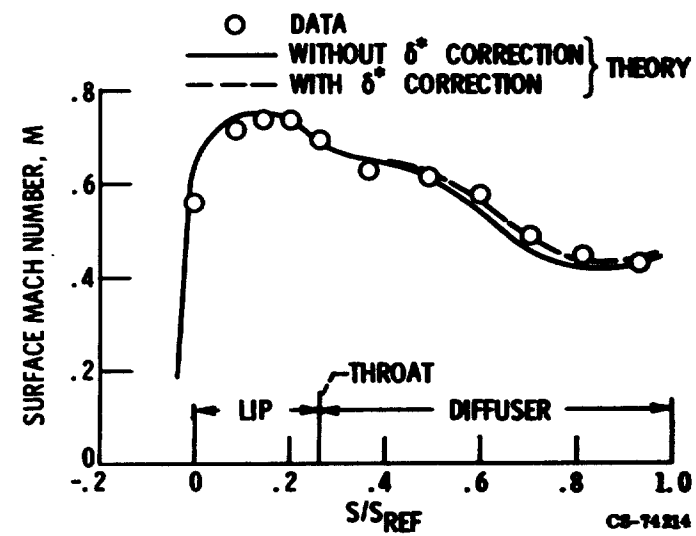

(b) BOUNDARY LAYER ATTACHED, $\alpha = 0$.

Figure 11. - Inlet with boundary layer, $M_{th} = 0.50$, $M_\infty = 0.13$.

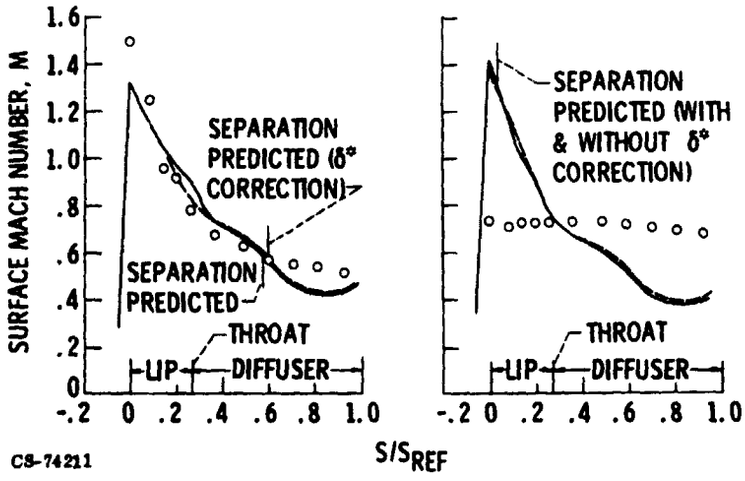

(c) DIFFUSER SEPARATION, $\alpha = 40^0$.

(d) LIP SEPARATION, $\alpha = 50^0$.

Figure 11. - Concluded.

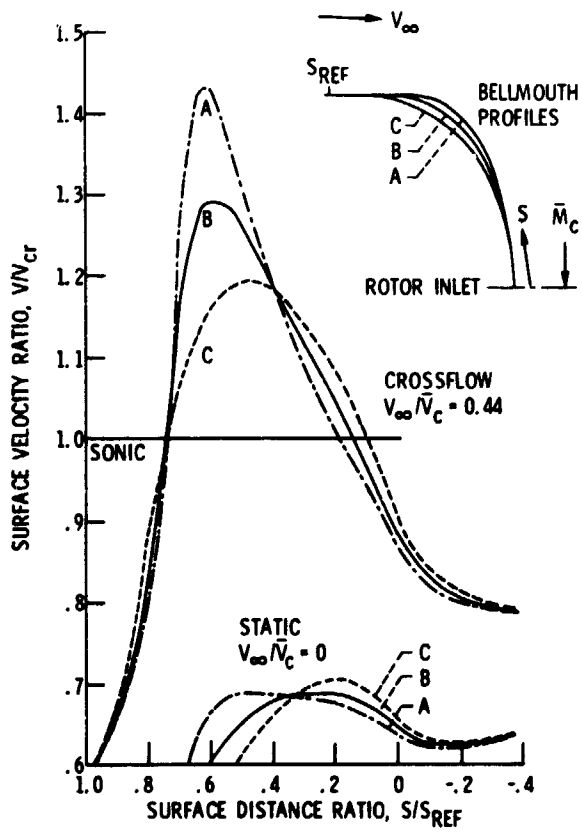

(a) SURFACE VELOCITY DISTRIPUTION.

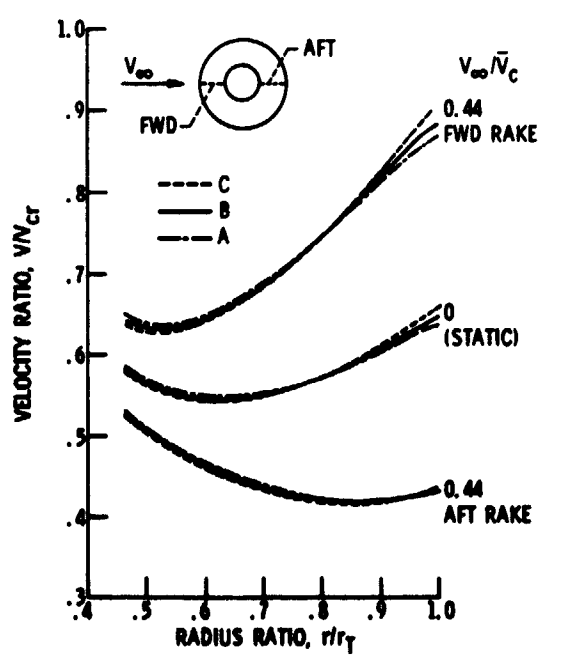

(b) FAN FACE VELOCITY PROFILES.

Figure 12. - Application of theory to VTOL inlet design. Average rotor inlet Mach number, $\bar{M}_c = 0.53$.

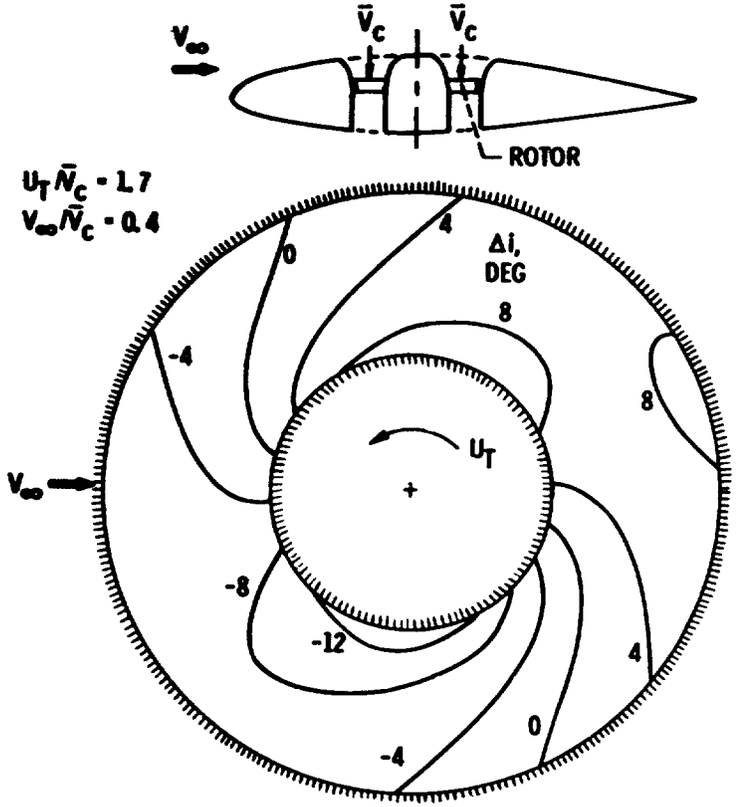

Figure 13. - Application of theory to VTOL inlet analysis. Rotor inflow distortion in crossflow.

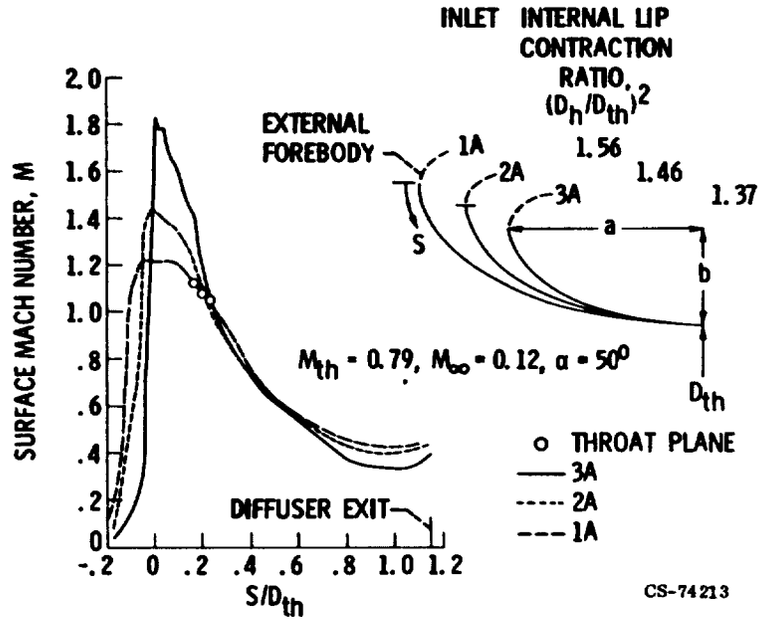

Figure 14. - Effect of internal lip contraction ratio on surface Mach number distribution.

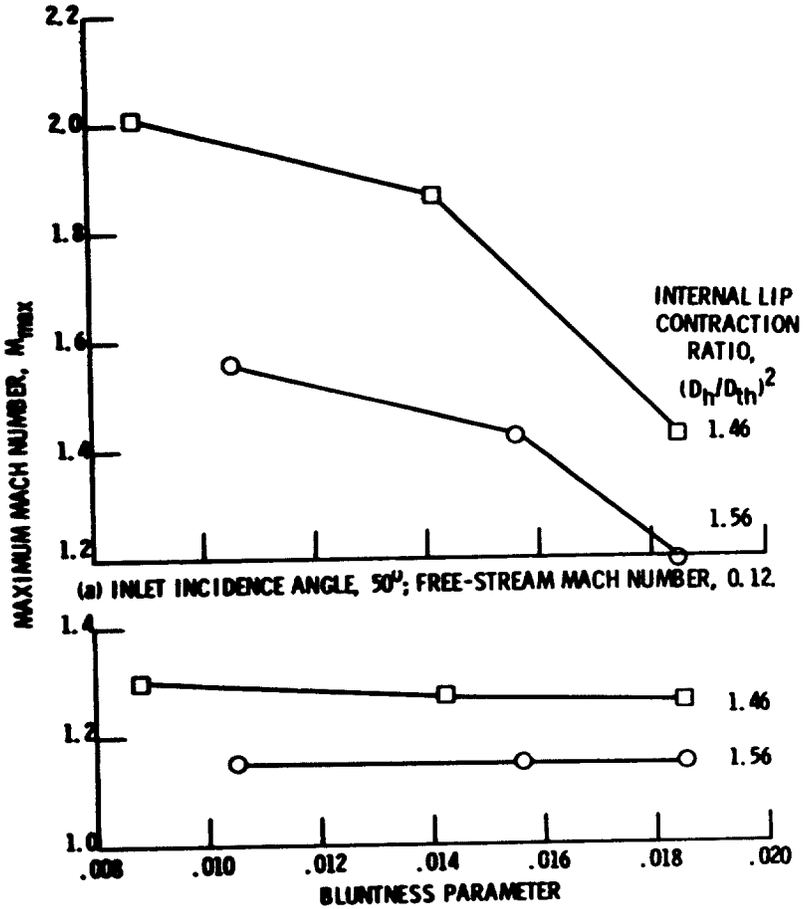

(a) INLET INCIDENCE ANGLE, 50°; FREE-STREAM MACH NUMBER, 0.12.

(b) INLET INCIDENCE ANGLE, 30°; FREE-STREAM MACH NUMBER, 0.18.

Figure 15. - Effect of external forebody bluntness parameter on maximum internal surface Mach number on windward side of inlet. One-dimensional throat Mach number, 0.79.

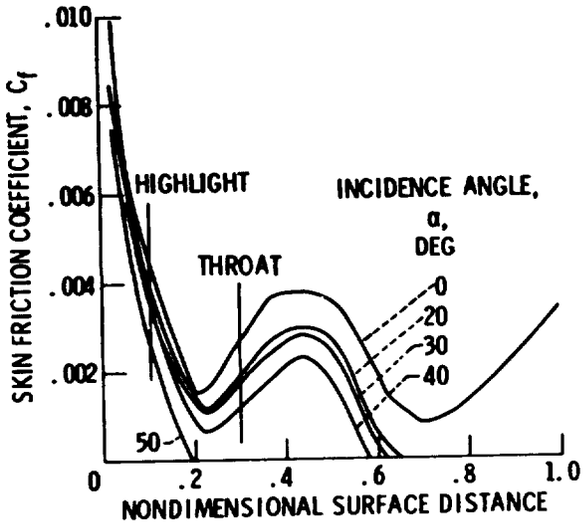

CS-74212

Figure 16. - Theoretical skin friction coefficients (without boundary-layer correction) for inlet of figure 11(a). One-dimensional throat Mach number, M_{th}, 0.50; free stream Mach number, M_∞, 0.13; windward side of inlet.

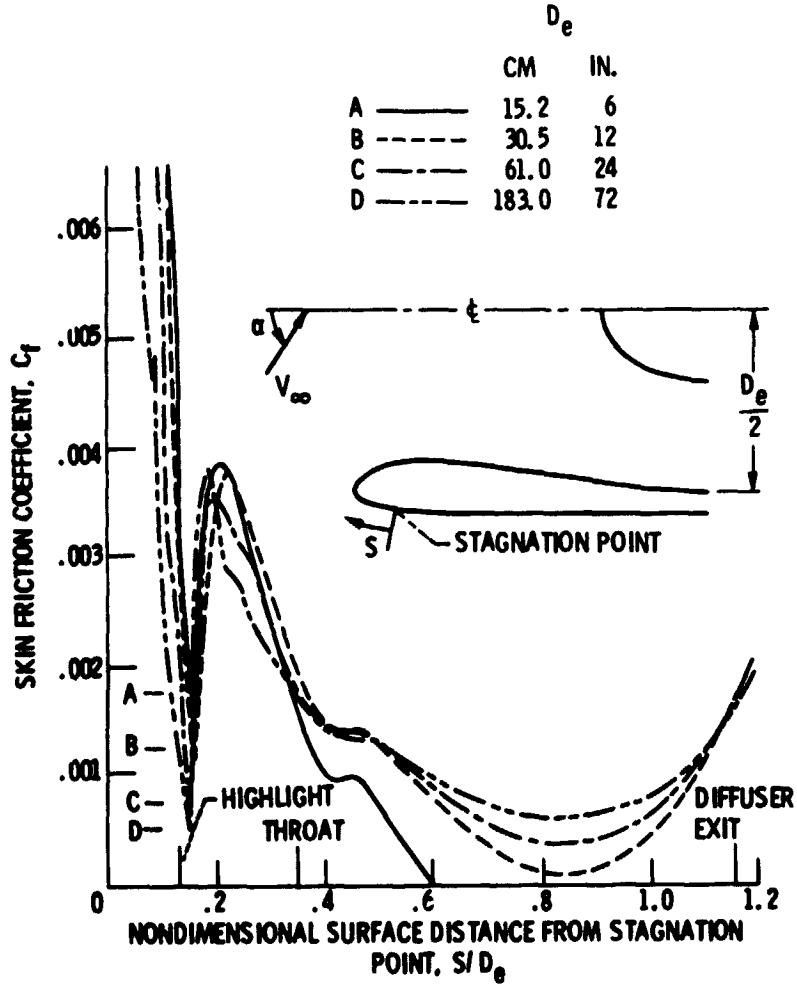

Figure 17. - Effect of scale on skin friction coefficient distribution on windward side of STOL engine inlet. $M_{th} = 0.28$, $M_\infty = 0.13$, $\alpha = 41^0$.